Hydraulic Fracture Propagation in Unconventional Reservoirs: The Role of Bedding Plane

Suling Wang[1], Yang Li[1], He Liu[2] and Minzheng Jiang[1]

Abstract: Hydraulic fracturing is a widely used technology in stimulation of unconventional reservoirs to obtain commercial production. Meanwhile, the bedding plane between sandstone and mudstone is a key challenge in unconventional reservoirs especially. During hydraulic fracture propagation, any diversion or abrupt change in hydraulic fracture path caused by bedding plane, leads to job failure.

In this paper, presents a numerical simulation method for a growth of hydraulic fracture interacting with a geological discontinuity in bedding plane. A 3-D hydraulic fracture model has been developed that can consider the elastic-plastic rock deformation coupled to fluid flow. The fracture growth is modeled by the damaged plasticity model of the continuum medium. The injection fluid flow rate value is given by the subroutines. This paper gives out a engineering example using the method to computer. The numerical calculation results coincide with test results which are microseismic data of a fracture propagation. The bedding plane between sandstone and mudstone can result in fracture blunting, crossing or entering the interface. The numerical results indicate that hydraulic fracture diversion is controlled strongly by the shear strength of the discontinuity, as well as the mechanical property. It is clearly observed that the larger differences of the mechanical property is more easily to deflection, due to the interfacial shear deformation increases. Once the shear stress is larger than the shear strength of the interface, the fracture tip become blunting and failure along the interface. So the fracture growth pattern depends on the shear strength of the interface and the stress contrasts.

The hydraulic fracturing methods that include interfacial properties can be used to better simulate fracturing in bedding plane, and it is important to improve fracture design and evaluation in unconventional reservoirs.

Keywords: Hydraulic Fracture, Fluid-Structure Interaction, Bedding Plane, Damaged Plasticity Model, Fracture Propagation.

[1] School of Mechanical Technology and Engineering, Northeast Petroleum University, Daqing, China. Email: wsl19751028@163.com

[2] Research Institute of Petroleum Exploration and Development,CNPC,Beijing,China.

1   Introduction

Hydraulic fracturing is a widely used technology in stimulation of unconventional reservoirs to obtain commercial production. The prediction of hydraulic fracturing geometrical form is the main factor to evaluate the effects of hydraulic fracturing.

It is very important to establish mathematical model for hydraulic fracturing accurately. The establishment of fracturing mathematical model can date back to the 1950s, after fifty years of development, from the original relatively simple 2-D model KGD [Perkins et al. (1961)] and PKN [Geertsma et al. (1969)] develop to the quasi three-dimensional (P3-D) model [Vandamme et al. (1989)] which is more closer to reality, the disadvantage of this approach is the derivation of the equation for fracture width is adopts the 2-D linear-elastic theory mostly, failing to reflect the fully three-dimensional deformation of rock, and suppose that the fracture extension direction is invariable, without consideration of fluid-solid coupling effect between fracturing fluid and rock pore medium, the fluid within fracture is one-dimensional flow. It is not applicable for the low permeability, thin and poor reservoirs development. Low permeability,thin and poor reservoirs have low porosity, low permeability, low oil saturation,as well as poor lithology and physical property characteristics. The reservoirs not only more but also thin,and in the same layer the lithology properties, physical properties and in-situ stress are different. Hydraulic fracturing in the thin and poor reservoir formed the main fractures, at the same time produced secondary fractures, due to the effect of bedding plane between sandstone and mudstone, fracture maybe divert during propagation process, or expand in height and get into the mudstone layer.

Hydraulic fracture propagates in the vertical has been investigated since the 1980s, Cleary [Cleary (1980)] and Daneshy [Daneshy (1978)] research shows:in-situ stress difference between reservoir and interlayer, modulus of elasticity difference, fracture toughness difference, interface strength, and fracturing fluid pressure distribution and rheology in fracture, all of those will have an important effect on the extension of fracture in the vertical.

The United States laboratory [Anderson (1981)] experiment studies the interface strength between reservoir and interlayer has influence to the extension of fracture in the vertical.In their opinion only in shallow formations, interface shear strength between reservoir and interlayer is the factor to influence the extension of fracture in the vertical. When the interface strength is large enough, fracture whether or not propagate into the interlayer, have relationship with the rock mechanical property difference between reservoir and interlayer.

Ali Daneshy [Daneshy (2009)] through the coal fracture analysis in the interface, separately adoption of pressure difference between reservoir and interlayer or mod-

ulus of elasticity difference, can not be taken as extension condition to judge fracture height, it's have relationship with the interface mechanical property between reservoir and interlayer, when due to interfacial shear slip engenders deformation, fractures will get blunt, the propagation of fracture in height is restrained, and lead to fracture width and length increases, but Ali Daneshy does not point out the mechanics essence of this phenomenon.

The above to fracture height propagation research mainly adopts experiment and theoretical study, theoretical research is limited to quasi three-dimensional (P3-D) hydraulic fracture, and along with the extension of application scope of hydraulic fracturing technology, urgent need fully three-dimensional (3-D) hydraulic fracture prediction technology, considering fracture extension rule under heterogeneous geological conditions. In this study, we adopt Abaqus (6.10), 3-D elastic-plastic finite element numerical simulation of consolidation are employed to model hydraulic fracturing process of oil reservoir.

Combined with the formation process of hydraulic fracture, the rock deformation consolidation process is regarded as a fluid-solid coupling multi-physics field elastoplastic problems, this analysis employs the D-P rock yielding criterion. This paper studies hydraulic fracture propagation pattern under the different bedding plane shear strengths, the different initial in-situ stress states, different rock mechanical property parameters. The result can provide a theoretical foundation for low-permeability thin and poor reservoir effective development.

2   Fracture extension prediction method

2.1   *Pore fluid diffusion/deformation equations*

Rock mass which consists of pores was taken as porous continuum. Under the fracturing fluids force, its hydrodynamic response is a typical problem of fluid-solid coupling. The complicated structure of underground flow-solid system determined that the mathematical model can be consider as a set of nonlinear, unstable state, multiphase flow solid coupled partial differential equations. It is the key to resolving the problem, which adopting effective numerical method to transform mathematical model into discrete solution.

The mathematical equations are discreted use of Galerkin method, through the general finite element method to calculate the element stiffness and construction stiffness assembly, getting the governing equations of pore fluid diffusion/deformation as in (1):

$$\begin{bmatrix} K_{dd} & K_{du} \\ K_{ud} & K_{ff} \end{bmatrix} \begin{bmatrix} u \\ p \end{bmatrix} = \begin{bmatrix} F_d \\ F_f \end{bmatrix} \tag{1}$$

Where u is the displacement of reservoir rock mass; p is the fluid pressure; K_{dd} is the displacement stiffness matrix; K_{ff} is the pressure of matrix; K_{du} and K_{ud} is the stress and pore coupled matrix; F_d and F_f is the external load matrix.

Solving equation(1), K_{dd} is far more than K_{ff} due to Young's modulus and Permeability coefficient lead to larger calculation error,so generally decompose into two soliton equations solution respectively is given by:

$$K_{dd}u = F_d - K_{df}p \tag{2}$$

$$K_{ff}p = F_f - K_{df}^T u \tag{3}$$

In the stress equilibrium condition equations, total stress σ is consist of effective stress σ' and osmotic pressure p as in (4):

$$\sigma = D\varepsilon - P'I \tag{4}$$

Osmotic pressure is equivalent to an initial stress, and it is added into the finite element equation as an initial stress load coefficient which is amount to equivalent osmotic load which is given by:

$$R_p = \int_e B^T p' I dxdydz \tag{5}$$

The effect of the strain rate on the fluid motion functions is takes as source, the element equivalent strain rate load is as in (6):

$$-\iiint_e v_i(\partial\varepsilon/\partial t)dxdydz \tag{6}$$

Adding this load into element load in the general unsteady flow program will be complete fluid part of fluid-structure coupling application. By introducing a time integration operator in the pore fluid flow equation and using the Newton linearization, these equations form the basis of the iterative solution of a time step which is found. The approach is to solve the coupled systems directly to get the stress distribution of rock mass.

2.2 *Damaged plasticity model for rock mass*

Fracture extension is based on damaged plasticity model. An additive strain rate decomposition is assumed for the rate-independent model as in (7):

$$\dot{\varepsilon} = \dot{\varepsilon}^{el} + \dot{\varepsilon}^{pl} \tag{7}$$

where $\dot{\varepsilon}$ is the total strain rate; $\dot{\varepsilon}^{el}$ is the elastic part of the strain rate; and $\dot{\varepsilon}^{pl}$ is the plastic part of the strain rate. It assumed that the elastic part of the strain is always small, so this equation can be integrated as in (8):

$$\varepsilon = \varepsilon^{el} + \varepsilon^{pl} \tag{8}$$

Damaged states in tension and compression are characterized independently by two hardening variables, $\tilde{\varepsilon}_t^{pl}$ and $\tilde{\varepsilon}_c^{pl}$, which are referred to as equivalent plastic strains in tension and compression respectively. Micro-fractureing and crushing in the concrete are represented by increasing values of the hardening variables. These variables control the evolution of the yield surface and the degradation of the elastic stiffness. They are also intimately related to the dissipated fracture energy which is required to generate micro-fractures.The stress-strain relations are governed by scalar damaged elasticity as in (9):

$$\sigma = (1-d) D_0^{el} : \left(\varepsilon - \varepsilon^{pl} \right) \tag{9}$$

where D_0^{el} is the initial (undamaged) elastic stiffness of the material; d is the scalar stiffness degradation variable, which can take values in the range from zero (undamaged material) to one (fully damaged material). Damage associated with the failure mechanisms of the rock mass (fractureing and crushing) therefore results in a reduction in the elastic stiffness.

3   Finite element models

3.1   Geometry model

The geometry model is related to the geological structure. It includes the thickness of sandstone and mudstone and the burying deepness. These can be got by the ground stress measurement. The ground stress distributions are different for the different wells. In this study, well #XI03-61 in Hailaer Basin is analyzed for predict fracture shape by using proposed method. Fig. 1 is the ground stress measurement curve of the well #XI03-61.The pay zones which lie at depths of between 2257.6m and 2260.4m is tuffaceous sandstone reservoir with low permeability. Because the minimum horizontal stress value is larger and the natural gamma ray value is larger, so the upper 2257.6m $\sim$ 2254m place and the bottom 2260.4m $\sim$ 2277m place are the interlayer.

This study is primarily focused on investigating the fracture extension. The geometry model take form the fracturing layer. The section of the model is shown in Fig. 2. The thickness of the model is 40m, the radius of the model is 75m.

Ground stress interpretation result diagram of well
#XI03-61 in Daqing oil recovery engineering institute
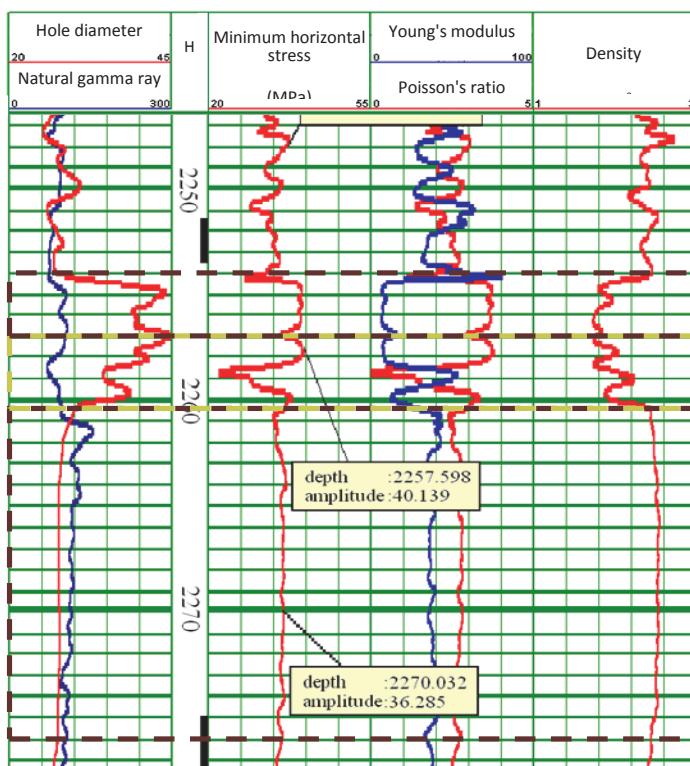
Figure 1: The ground stress measurement curve of well #XI03-61.
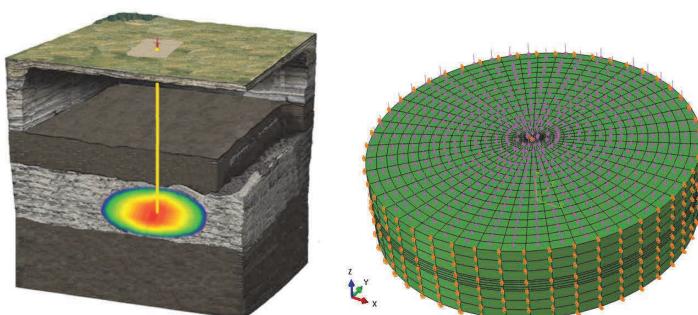
Figure 2: The finite element model of well XI03-61.

3.2 The bedding plane

The bedding plane is formed through the geological formations. It has two features. The large changes in material properties (such as Young's modulus and Poisson's ratio) mean that the two layers at the interface can not deform the same amount. If the bonding between the two adjacent formations is weak, shear failure occurs along the interface. In a strong bonding interface absence of slippage simply means that the shear stresses are not large enough to cause failure. Presence of shear stresses means the interface also means a change in the orientation. The other change is the in-situ state of stress. The in-situ state of stress is created by the regional tectonic stresses. With each layer, formation in-homogeneity causes local stress contrasts. The stress contrasts are larger, fractures are not easier to extend.

3.3 Property

The rock has the elastoplastic behavior under the high pressure. Material properties are defined as the damaged plasticity model. The plastic model uses the non-associative plastic flow rule, and the plastic potential function adopts the D-P model. The plastic-damage concrete model uses a yield condition based on the yield function proposed by Lubliner (et al. 1989) and incorporates the modifications proposed by Lee and Fenves (1998) to account for different evolution of strength under tension and compression. In this paper, the rock material properties should be given, and the other coefficients are default, which are shown in the Tab. 1.Boron guar gelled fracturing fluid was used in #XI03-61 well, leak off coefficient determined by the test is 7.8×10^{-4}m/min$^{1/2}$, preflush injection time is 510 seconds, the injection flow rate is 3.5 m^3/min.

Table 1: The material properties for rock.

	Young's modulus/GPa	Poisson's ratio	Density/kg.m^{-3}	Cohesion	Internal friction angle
Upper layers	7	0.42	1200	13.7	20.1
Pay zone	50	0.16	1700	26.4	28.3
Lower layers	38	0.35	2200	18.5	23.8

3.4   Boundary conditions and initial conditions

Zero-displacement constraints are given to the normal direction of all the external surfaces of the model. Constant pore pressure is given to the lateral surfaces. Initial conditions are given as follows: the initial pore pressure is set as 24.5 MPa, and the initial porosity is set as 0.17. The minimum horizontal stress can get by the ground stress measurement, and the vertical stress can calculate by the weight of the overlying rock layers. Gravity load is applied to the model. This gravity load will be used to balance the initial geostress field with the existence of pore pressure, and will be automatically modified by equilibrium equations.The detail geostress parameters are shown in Tab. 2.

Table 2: Initial geostress parameters of well #XI03-61

	Vertical stress /MPa	Maximum horizontal stress /MPa	Minimum horizontal stress /MPa
Upper layers	49.65	44.57	40.13
Pay zone	49.69	28.88	26.00
Lower layers	49.72	40.00	36.28

4   Well #XI03-61 simulation results

With the model definition provided in Section 3, a coupled numerical simulation was performed. The calculation contains two steps: appling the gravitational field to form the initial geostress field and injecting the fracturing fluid to form the fracture. Numerical results are shown in Fig. 3 for the last step.

The distribution rule of pore pressure, porosity and the maximum principal stress are the same. Under the pressure of percolation flow, the rock porosity and pore pressure are increase, and cause the initial stress state of rock mass to redistribute. Where the pore pressure is bigger, the the major principal stress of rock mass is larger, the maximum principal stress is positive illustrate when the rock in tensile state. The red areas indicate that the rock under the action of tensile stress occur tensile damage.

Fig. 4 shows the state of distributed damage for the different stages. The injection nodes are selected according to the spiral perforation mode. Due to the fracture propagation along the formation of the maximum horizontal principal stress direction, the fracture first extend along the perforating eye in the fracturing initial

(a) The distribution of the pore pressure at the last step.

(b) The distribution of the porosity at the last step.

(c)The distribution of the maximum principal stress at the last of step.
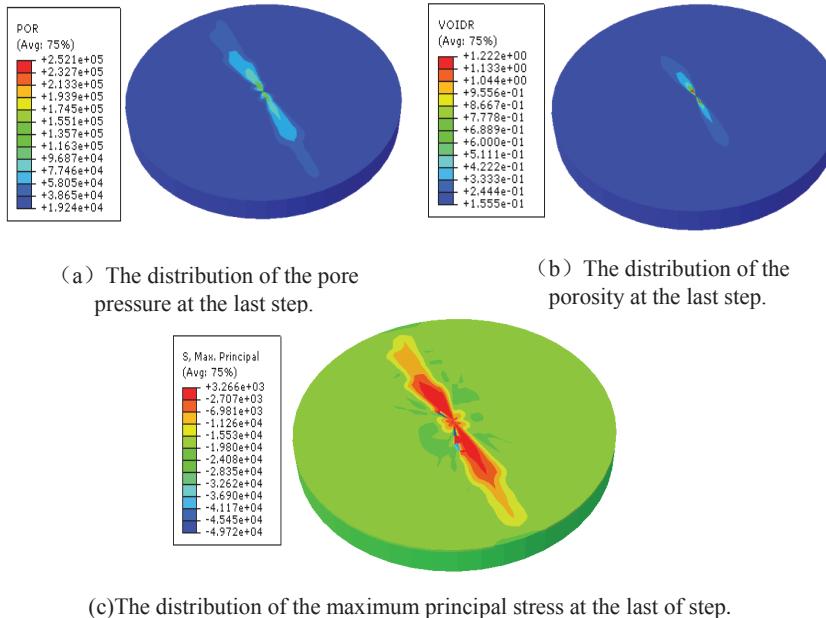
Figure 3: Numerical results for the injection sequence

stage, with the fracturing fluid injection, fracture propagation around the wellbore and radial direction extend gradually, last formed two symmetrical main fracture, the main fracture formation is similar to the distribution state of maximum principal stress.

In order to track the expansion of fractures, monitor fracturing process of #XI03-61 well by microseismic monitoring team. Fig. 5 shows fracture length monitoring results. The horizontal shaft along the east-west and the east is positive direction. The vertical shaft along the north–south and the north is positive direction. The red dot represents the fracture distribution state.The fracture is incomplete symmetry state about wellbore. The fracture length is up to 84 m in the northwest orientation, and reach to 46m in southeast orientation. The total length is 130m.

Fig. 6 shows the change of fracture height, the diagram shows fracture height not smooth, two wings front upward tilt. The fracture total height is 20m.

The test results of the fracture length and height have good consistency with the numerical simulation results. The test fracture height is 20m, fracture length is 130m, and numerical simulation fracture height is 18.5m, length is 119m, height error is 7.5%, length error is 8.4%, and this method has been proved to be right.

(a) t=50s

(b) t=200s

(c) t=350s

(d) t=510s
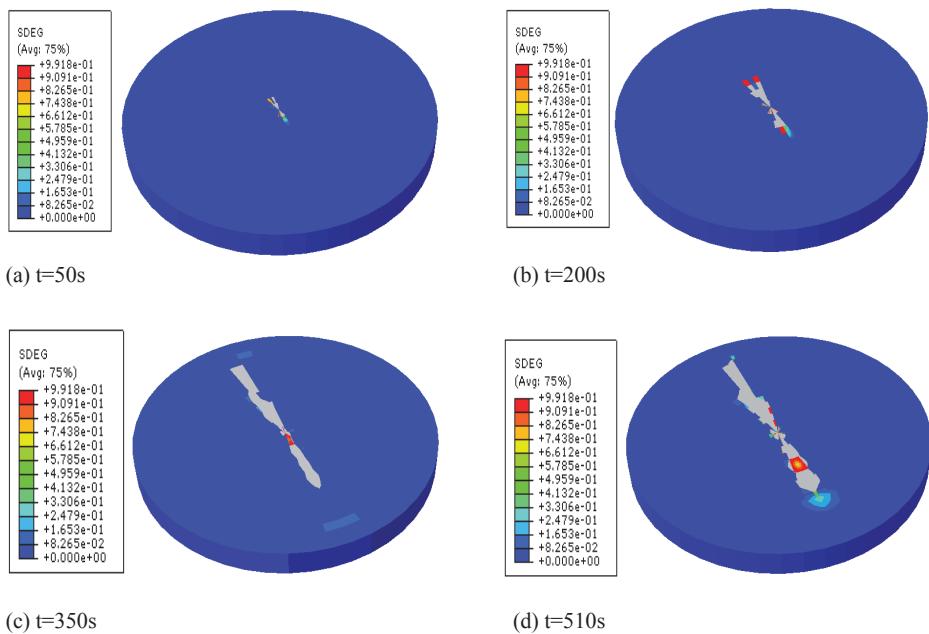
Figure 4: Damage results for the injection sequence
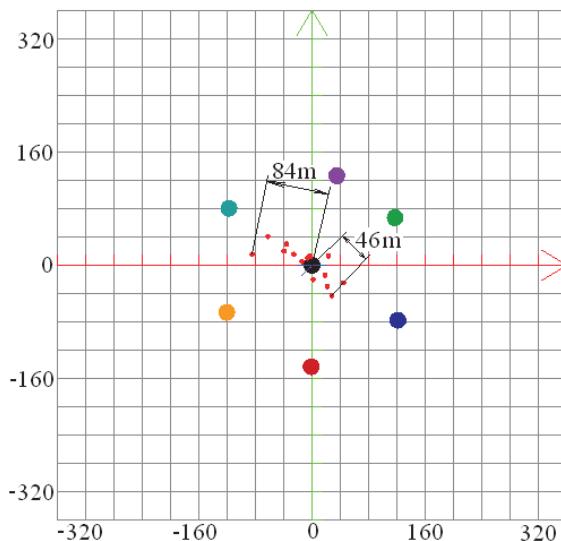
Figure 5: #XI03-61 well monitoring artificial fracture length.
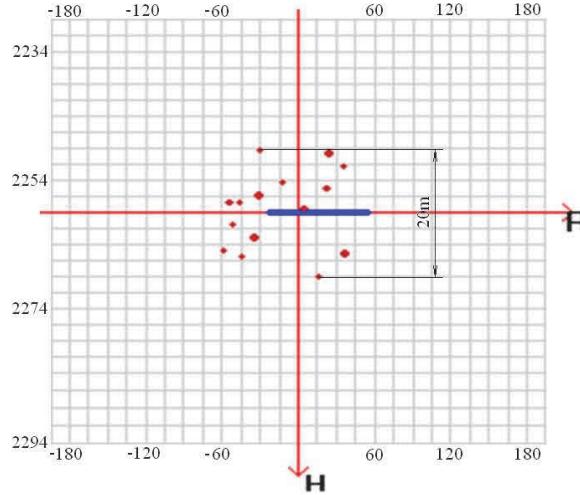
Figure 6: #XI03-61 well monitoring artificial fracture height.

5   Fracture propagation analysis

5.1   Case-1 The strength of bedding plane

Fig. 7 and Fig. 8 show fracture propagation under strong and weak bonding strength of bedding plane. Fig. 7 shows, hydraulic fracture crossing bedding plane, due to strong bonding strength. Compared to Fig. 7, weak bonding strength leads to hydraulic fracture entering into bedding interface propagation.

Fracture reorientation occurs when crossing the weak bonding strength bedding plane. With the fracture propagating towards interface, the yield of interface layer increases gradually which is lead to the increase of plastic strain. When the plastic strain of interface reaches the ultimate accumulated damage of the interface material, secondary fracture will occur on the weak bonding interface. It will causing interface debonding, meanwhile, the local stress field of fracture tip will become smaller, the trend of fracture tip expand is weakened and leads to fracture reorientation. The smaller interface bonding strength is, the larger the plastic strain of interface is, and the larger shear deformation occurs on the interface, the more likely to deflection of the fracture. Consequently, the main reason for fracture propagation reorientation caused by interface is shear deformation. The values of the variables along Path-1 are shown in Fig. 10.

Fig. 10 shows the value of the synthetic damage variable along the Path-1. The parameter "SDEG" is the equivalent parameter as the equation (9). When the parameter SDEG of element is approximate to 1, the element is damaged. From the
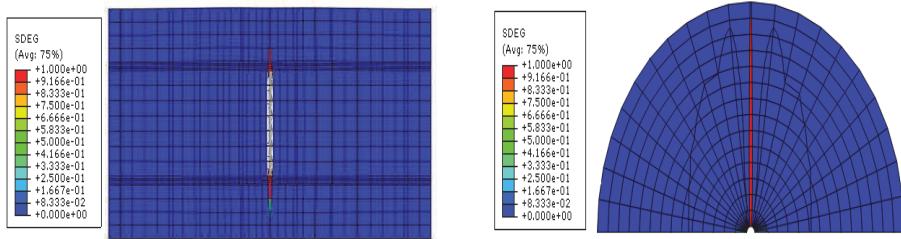
Figure 7: Hydraulic fracture propagation under strong bonding strength.
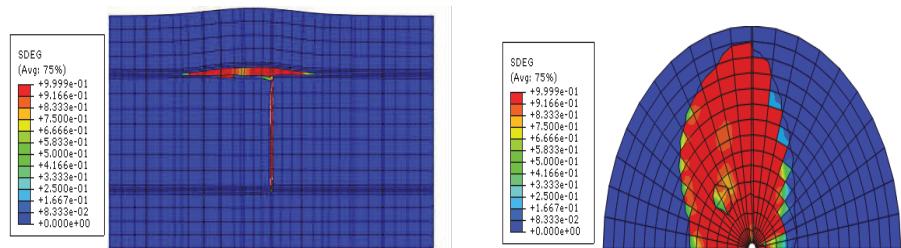
Figure 8: Hydraulic fracture propagation under weak bonding strength.
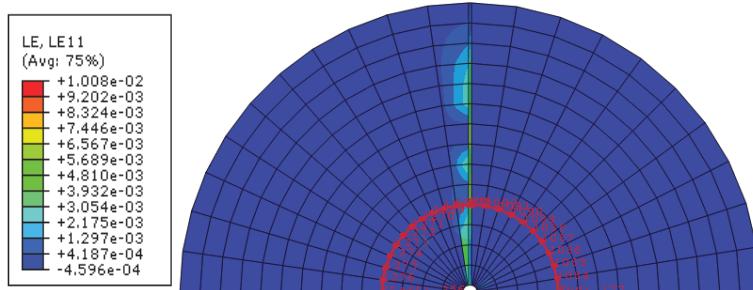
Figure 9: The illustration of Path-1.

Fig. 10, damage occur only in the center symmetric position under the strong bonding interface, and damage occur from 10m to 33m range under the weak bonding interface. It shows that the fracture extends within the interface layer.

The values of the strain ε_{xx} along the Path-1 are shown in Fig. 11. The strain localization band shows the vertical fracture position, and the values can show the fracture opening. The strain of strong bonding interface is larger than that of the weak bonding interface, which can show that the vertical fracture of the strong
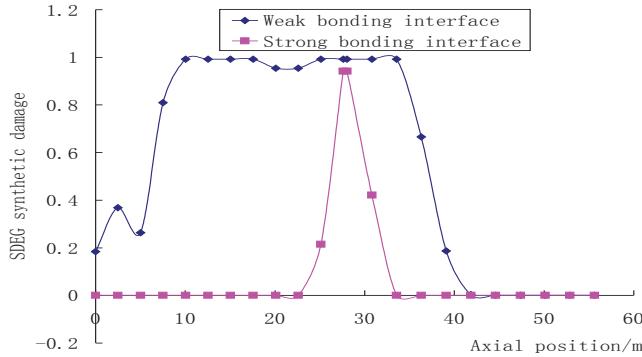
Figure 10: The distribution of synthetic damage along Path-1.
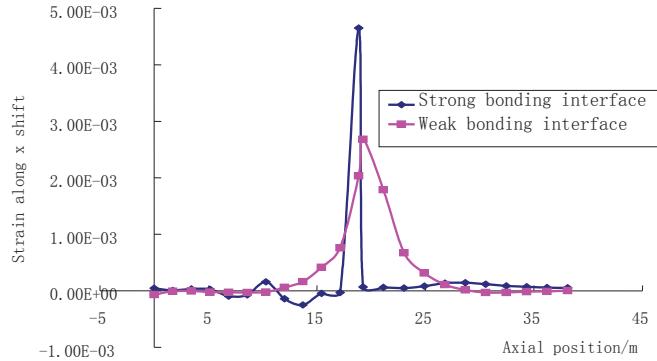
Figure 11: The distribution of ε_{xx} along Path-1.

bonding interface is more likely to pass through the bedding plane, due to the damage of weak bonding interface, the vertical fracture of weak bonding interface may be deflect.

Fig. 12 and Fig. 13 show the shear strain variation in different interface bonding strength.

Fig. 12 shows the distribution of shear strain ε_{xz}, the shear strain direction is perpendicular to the Z-axis and along the horizontal direction, compared with Fig. 10, where the value of synthetic damage of the interface is larger, the shear strain is larger at the same time, which can show the shear strain increases led to the damage of the interface, and it is more likely to occur in the weak bonding interface.

Fig. 13 shows the distribution of shear strain ε_{xy}. The shear strain direction is perpendicular to the Y-axis along the horizontal direction, the displacement of Y-
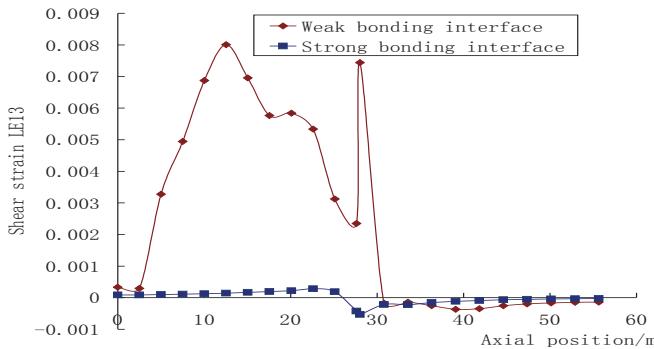
Figure 12: The distribution of ε_{xz} along Path-1.
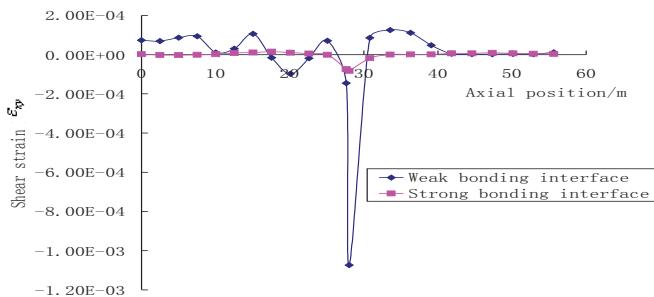
Figure 13: The distribution of ε_{xy} along Path-1.

direction has less affected by fracture opening extension, therefore, shear strain ε_{xy} has less affected by interface bonding strength. Compared to Fig. 12, the value of the ε_{xy} is significantly less than the ε_{xz}.

5.2 Case-2 The Property of reservoir

The state of stress near interface between sandstone and mudstone is much more complex. It causes by the material properties(such as Young's modulus and Poisson's ratio).It means that the two layers at the interface can not deform at the same amount. The shear stress will be occured along the interface. All the values of parameters be used here are the same as those used previously, except the change of the in-situ state of stress, the Young's modulus and Poisson's ratio.

The Fig. 14 is the shear stress distribution of the bedding plane along the X-direction. The Fig. 15 is the shear stress distribution along the Path-1.The three curves are obtained under the condition which the Young's modulus of sandstone is 2×10^{4}MPa and the Young's modulus of mudstone is 1×10^{4}MPa, 5×10^{3}MPa
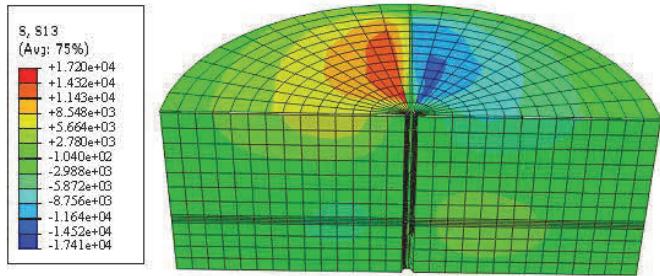
Figure 14: The symmetric distribution of s_{xz} at the bending.
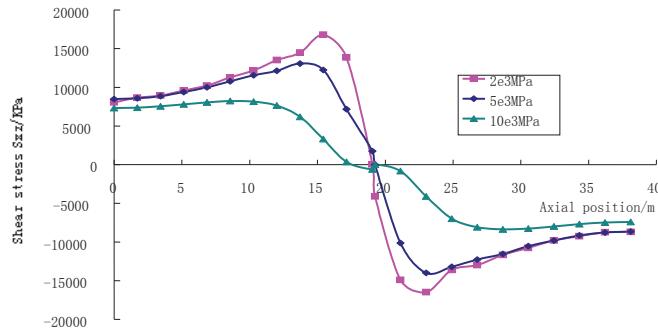
Figure 15: The distribution of s_{xz} along the Path-1.

and 2×10^3 MPa separately. In order to contrast, the in-site state of stress contrasts is 5MPa.

From the Fig. 14. It can be find that the larger difference of the mechanical property of sandstone and mudstone, the greater of interface deformation difference in the interface between sandstone and mudstone.

Fig. 14 illustrates the distribution of shear stress is symmetric, and it shows the fracture expand symmetrically under the action of internal pressure when set the sandstone and mudstone as the same material. The maximum difference is less than 0.3 MPa between two ends, and so it is difficult to cause fracture propagation deflection.

The shear deformation on one end is bigger, it makes the opening mode fracture propagation translated into mixed mode fracture propagation with opening mode and shear mode. The larger interface asymmetric shear deformation, fracture propagation is prone to shear damage failure.

Set the material properties between two end of fracture is different, Young's mod-
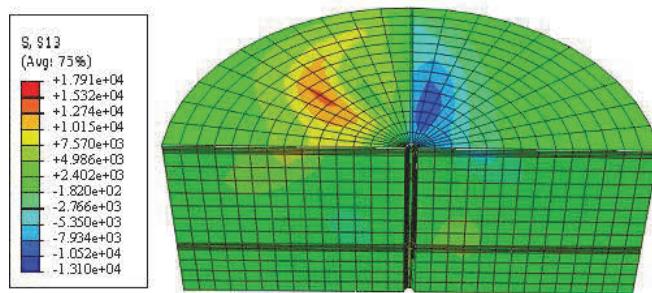
Figure 16: The asymmetric distribution of s_{xz} at the bending.
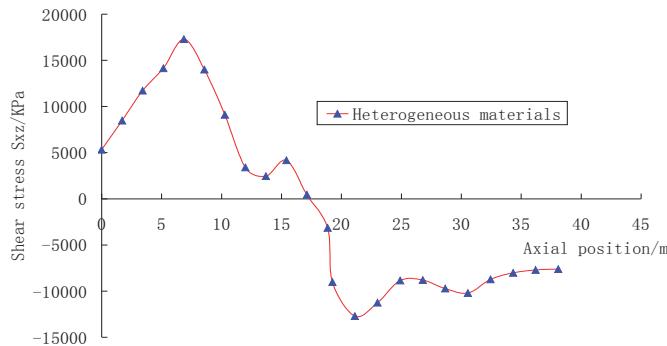
Figure 17: Distribution of s_{xz} along the Path-1 with the heterogeneous material.

ulus of sandstone on the left end is 2×10^3 MPa and on the right end is 5×10^3 MPa. Fig. 16 is the distribution of the shear stress s_{xz}. It shows that the shear stress between two ends of fracture is asymmetric.

The Fig. 17 is the shear stress distribution along the Path-1. In the Fig. 17, the maximum difference between two ends is 4.56MPa, and the position of the maximum shear stress is difference. It shows the shear deformation on one end is larger than the other one. It makes the I mode fracture opening propagation translated into I-II mixed mode fracture propagation. Along with the asymmetric shear deformation in the interface increasing, the fracture propagation is prone to engender shear failure damage.

According to the contrast between Fig. 16 and Fig. 14, the mudstone material between two ends of fracture is different, the larger difference in mechanical property of sandstone and mudstone, resulted in the shear stress will larger and the fracture propagation deflection will happen sooner.

Fig. 18 and Fig. 19 is a comparison of two cases on fracture propagation. The fracture propagation deflection is easy to happen when one end shear stress is larger.

Minimum horizontal stress difference of sandstone and mudstone is one of the main factors which affecting the fracture propagation. The minimum horizontal stress of mudstone is larger than sandstone, increasing the critical load of fracture extending in the mudstone, the interaction can result in fracture blunting, as shown in Fig. 18. If the sandstone and mudstone minimum horizontal stress difference is smaller, the fracture can pass through the bedding plane and get into the mudstone, but the orientation of fracture propagation doesn't change, as shown in Fig. 7. Fracture re-orientation is depends on the interfacial bonding strength and sandstone/mudstone mechanical property difference. When the sandstone and mudstone mechanical property difference became smaller, interfacial bonding strength became larger, the fracture is easy to crossing the interface.
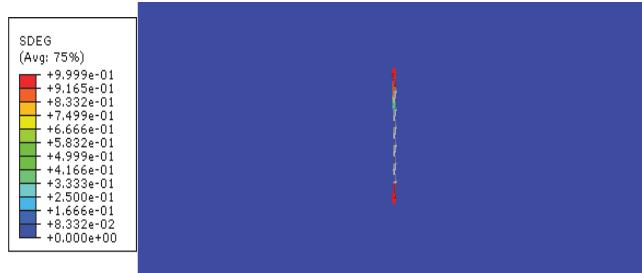
Figure 18: Fracture ends material symmetry.
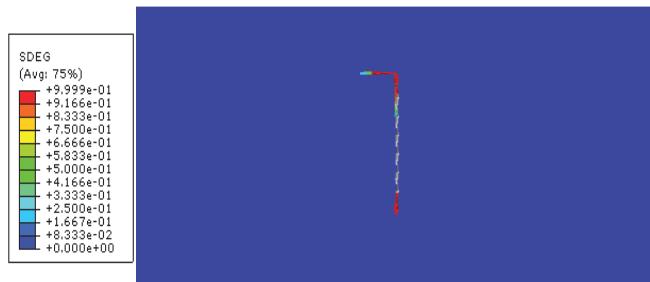
Figure 19: Fracture ends material unsymmetry.

6 Conclusions

Based on values of the material used in the model, the fracture length of well XI03-61 is the 119.8m and the height is 18.5m. This test fracture length with measured microseismic data is 130m and the height is 20m, the error of fracture height is 7.5%, the error of fracture length is 8.46%. The numerical simulation example shows the damaged plasticity model of the continuum medium can describe the fracture propagation.

The main factor which influence the propagation orientation of fracture is the shear strength of bedding plane. In the same conditions, the shear strength of weak interface has the relatively poor ability to resistance the interface shearing deformation, and is more likely to occur shear failure which result in the interface laminating or splitting. Shear failure results in the blunting of the fracture tip and completely stops its local growth. On the other hand, the fracture is more likely to through the interface if the interface is strong bonding strength. The deflection angle of the fracture is depended on the shear strength of sandstone and mudstone interface layer.

Initial in-suit stress difference of reservoir rock is caused by the rock mechanical property difference during the process of geological structure. The mechanical property difference of sandstone and mudstone is larger, the larger shear deformation will occur when fracture through the sandstone and mudstone interface. Once the shear strain in the interface exceeds the interface tolerance and leds to the interface damage. The shear damage can result in fracture tip blunting and stopping to extend. The calculation results show that the fracture can deflect when the difference of Young's modulus reach the 1.3×10^4MPa. The value of minimum horizontal stress difference don't change the propagation orientation of fracture. It only influence the height of fracture.

References:

Abaqus Analysis User's Manual.Version 6.10.

Anderson, G. D. (1981): Effects of Mechanical and Frictional Rock Properties on Hydraulic fracture Growth Near Unbounded Interfaces. SPE:8347.

Cleary, M .P. (1980): Analysis of Mechanics and Procedures for Producing Favorable Shapes of Geometry of Hydraulic Fractures. SPE:9260.

Cheng, Y.; Shen, H.; Zhao, Y. et al. (2010): Study on fluid solid coupling of physical variation of gas hydrate reservoirs during natural gas development. *Acta Petrolei Sinica,* vol. 31, no. 4, pp. 607–611.

Dam, D. B.; Papanastasiou, P.; Pater, C. J. (2002): Impact of rock plasticity on hydraulic fracture propagation and closure. *Prod Facil*, vol.17,no.3,pp.149-159.

Daneshy, A. A. (1978): Hydraulic Fracture Propagation in Layer Formations. SPE:6088.

Daneshy, A. (2009): Factors Controlling the Vertical Growth of Hydraulic Fractures. SPE:118789.

Geertsma, J.; Klerk, F. De. (1969): A rapid method of predicting width and extent of hydraulically induced fractures. *Journal of Petroleum Technology*, vol. 21, no. 12, pp. 1571–1581.

Hillorberg, A.; Modeer, M.; Petersson, P. E. (1976): Analysis of crack formation and crack growth in concrete by means of fracture mechanics and finite elements. *Cement Concrete Res.* vol. 6, pp. 773–782.

Lubliner, J.;Oliver, J.; Oller, S.; Onate, E. (1998): A plastic damage model for concrete. *Int.J.Solids Struct.*, vol. 25, no. 3, pp. 299–326.

Perkins, T. K.; Kern, L. R. (1961): Widths of hydraulic fractures. *Journal of Petroleum Technology*, vol. 13, no. 9, pp. 937–949.

Shen, X. (2010): Subsidence Prediction and Casing Integrity With Respect to Pore-Pressure Depletion With 3-D Finite-Element Method.SPE:138338.

Shen, X.; Cullick, A. S. (2012): Numerical Modeling of Fracture Complexity with Application to Production Stimulation. SPE:151965.

Vandamme, L.; Curran, J. H. (1989): A three-dimensional hydraulic fracturing simulator. *International Journal for Numerical Methods in Engineering*, vol. 28, no. 4, pp. 909–927.

Xu, X. P.; Needleman, A. (1994): Numerical simulations of fast crack growth in brittle solids. *Mech Phys Solids,* vol. 42, no. 9, pp. 1397–1434.

Zhang, X.; Jeffrey, R. G.; Thiercelin, M. (2006): Deflection and Propagation of Fluid-Driven at Frictional Bedding Interfaces:a Numerical Investigation. *Structural Geology*, vol. 29, pp. 396–410.